Computer Vision and Image Understanding 115 (2011) 1062–1072

Contents lists available at ScienceDirect

Computer Vision and Image Understanding

journal homepage: www.elsevier.com/locate/cviu

2.5D Elastic graph matching

Stefanos Zafeiriou *, Maria Petrou

Imperial College, Department of Electrical and Electronic Engineering, London, UK

ARTICLE INFO

Article history:
Received 29 November 2009
Accepted 1 December 2010
Available online 17 March 2011

Keywords:
Elastic graph matching
3D face recognition
Multiscale mathematical morphology
Geodesic distances

ABSTRACT

In this paper, we propose novel elastic graph matching (EGM) algorithms for face recognition assisted by the availability of 3D facial geometry. More specifically, we conceptually extend the EGM algorithm in order to exploit the 3D nature of human facial geometry for face recognition/verification. In order to achieve that, first we extend the matching module of the EGM algorithm in order to capitalize on the 2.5D facial data. Furthermore, we incorporate the 3D geometry into the multiscale analysis used and build a novel geodesic multiscale morphological pyramid of dilations/erosions in order to fill the graph jets. We show that the proposed advances significantly enhance the performance of EGM algorithms. We demonstrate the efficiency of the proposed advances in the face recognition/verification problem using photometric stereo.

1. Introduction

Dynamic link architecture (DLA) was proposed as an abstract methodology for distortion invariant object recognition by Lades et al. [21]. In DLA, an object is represented as a connected graph. Each graph node is located at a certain spatial image location **x**. A feature vector, the so called jet, should be attached at each graph node. The jet elements can be local brightness values that represent the image region around the node. However, it is desirable to have more complex types of jet that are produced by multiscale image analysis by Lades et al. [21]. The representation of an object in DLA can be summarized in the following steps.

- Group all the features that correspond to the same graph node of the object into a jet.
- Group all the nodes and jets that belong to the object in order to form the object graph.
- Define neighborhood relationships for each graph node.

One of the most well-studied implementations of DLA is the elastic graph matching (EGM) algorithm. In Lades et al. [21] EGM was initially proposed for arbitrary object recognition from images and was a very popular topic of research for various facial image characterization applications. In EGM, a reference object graph is created by overlaying a rectangular elastic sparse graph on the object image and then calculating a Gabor wavelet bank response at each graph node. The graph matching process is implemented by the stochastic optimization of a cost function which takes into account both jet similarities and grid deformations. One of the basic advantages of EGM algorithms is that they can be applied in a fully automatic manner when combined with a face detector and/or a fully automatic facial feature detection algorithm [47,33,46].

1.1. EGM literature review

A lot of research was conducted in order to boost the performance of EGM for face recognition, face verification, facial expression recognition and sex determination [48,39,38,40,8,24,17,19,18,36,45,33,32,20]. In Wiskott et al. [39], the graph structure was enhanced by introducing a stack-like structure, the so-called *bunch graph*, and was tested for face recognition. For every node in the bunch graph structure, a set of jets was measured for different instances of a face (e.g., with open or closed mouth, open or shut eyes). This way, the bunch graph representation could cover a variety of possible changes in the appearance of a face. In Wiskott [38], the bunch graph structure was used for determining facial characteristics, such as beard, the presence of glasses, or even a person's gender. In Zafeiriou and Pitas [42] a bunch graph structure was used for facial expression recognition.

In Duc et al. [8], EGM was proposed and tested for frontal face verification. A variant of the typical EGM, the so-called *morphological elastic graph matching* (MEGM), was proposed for frontal face verification and tested for various recording conditions [17,18]. In Kotropoulos et al. [17,19,18], the standard coarse- to-fine approach proposed in Duc et al. [8] for EGM was replaced by a simulated annealing method that optimizes a cost function of the jet similarity measures subject to node deformation constraints. Another variant of EGM was presented in Tefas et al. [36], where morphological signal decomposition was used instead of the standard Gabor analysis [8]. EGM with Gabor jets for facial expression

* Corresponding author.
E-mail addresses: s.zafeiriou@imperial.ac.uk (S. Zafeiriou), maria.petrou@imperial.ac.uk (M. Petrou).

1077-3142/$ - see front matter © 2011 Elsevier Inc. All rights reserved.
doi:10.1016/j.cviu.2010.12.008

recognition was proposed in Lyons et al. [24,23,25], Hong et al. [14], and Zhang et al. [49]. EGM with morphological feature vectors for facial expression recognition was proposed in Zafeiriou and Pitas [42].

Discriminant techniques were employed in order to enhance the classification performance of EGM. The use of linear discriminant techniques at the feature vectors for the extraction of the most discriminating features was proposed in Duc et al. [8] and Kotropoulos et al. [17,18]. Several schemes that aim at weighting the graph nodes according to their discriminatory power have also been proposed in Zafeiriou et al. [44], Kotropoulos et al. [17,18], Krüger [20], and Tefas et al. [35]. A combined discriminant scheme was proposed in Zafeiriou et al. [45,46], where discriminant analysis was employed in every step of elastic graph matching for face verification. The use of Fisher's Linear Discriminant Analysis (FLDA) for discriminant feature selection in the graphs for facial expression recognition was proposed in Lyons et al. [24]. In Lyons et al. [24,25], FLDA was applied in a graph-wise manner (i.e., the feature vectors that were used in FLDA were the set of graph jets), contrary to the methods in Kotropoulos et al. [17,18], Zafeiriou et al. [45], and Zafeiriou and Pitas [42], where node-specific discriminant transforms were calculated. Moreover, a series of discriminant techniques in graph-based representations with Gabor features were proposed in Guo and Dyer [13]. The methods in Guo and Dyer [13] have some resemblance to EGM but have not implemented an elastic graph matching procedure, since landmark selection and matching was manually performed. In Shin et al. [33,32] novel robust to in-plane rotation and scaling, Gabor-based features were proposed and a novel wrapping elastic graph matching procedure was introduced. Moreover, in Shin et al. [33] a novel kernel-based method for feature extraction was proposed and used for face recognition.

In the first EGM algorithm evenly distributed graphs placed over a rectangular image region [8,17,18,36,35] were used or graphs that were placed on preselected nodes that correspond to some fiducial facial points (e.g., nose, eyes, etc.) [24,39,38,14,23,49,25]. Intuitively, one may think that graphs with nodes placed at pre-specified facial landmarks may perform better than the rectangular graphs. However, such graphs are more difficult to be automatically applied, since they require a detection module to find the precise coordinates of the facial landmarks in the reference images or, in many cases, manual landmark annotation [13,24,39]. On the contrary, an evenly distributed rectangular graph is easier to be handled automatically, since only a face detection algorithm is required to find an initial approximation of the rectangular facial region [8,17,18,36,35].

Recently, research was conducted concerning the type of graph that is most appropriate for face verification and facial expression recognition. In Zafeiriou et al. [47], an algorithm that finds the optimal discriminant graph structure was proposed (optimal according to a discriminant criterion). The graphs proposed in Zafeiriou et al. [47] have nodes placed at discriminant facial landmarks. It was shown in Zafeiriou et al. [47] and in Zafeiriou and Pitas [42] that these graphs can be found in a fully automatic manner and have better recognition performance than the typical rectangular graphs in face verification and facial expression recognition, respectively. Research on the optimal graph structure has attracted the interest of other researchers too [15,12], where it was shown that graphs with nodes upon facial regions, that are indicated by ridge and valley operators, lead to better recognition performance in comparison with graphs with nodes placed at manually selected landmarks. Finally, another recent research work concerning EGM was presented in Eckes et al. [9]. In this paper, an EGM-based system was presented for object recognition in cluttered scenes under partial occlusion. For that task EGM was extended in order to treat stereo image pairs in order to increase matching robustness and disambiguate occlusion relations.

1.2. Motivation and contribution

All EGM based methods proposed so far do not take into consideration the 3D nature of the objects. Nowadays, the acquisition of 3D objects and faces is a relatively simple procedure due low cost devices that are now available. This reason made 3D face recognition a very rapidly growing research topic. The other reason that made 3D face recognition a popular research topic is that, although 2D face recognition systems can achieve good performance in constrained environments like in Messer et al. [26], they still encounter difficulties in handling large amounts of facial variations due to head pose, lighting conditions and facial expressions. However, the acquisition of 3D face geometry also has limitations, such as the presence of noise and difficult image acquisition [4]. For the acquisition of 3D data different techniques have been used, such as laser and structured light scanners [10]. The acquisition of 3D face data using these techniques is intrusive. For example most of the available databases that contain 3D faces, like FRGC [29], are based on the structure light technology (for example the 3D images were acquired by a Minolta Vivid 900/910 series sensor) which require the person to stay still for a couple of seconds. Another technique that does not depend so much on the user's cooperation is 3D acquisition using photometric stereo [1,3,2]. The actual model that we acquire from the available 3D acquisition techniques is a 2.5D model. 2.5D is a simplified 3D (x,y,z) surface representation that contains at most one depth value (z direction) for every point in the (x,y) plane.

In this paper we propose methods for exploiting the 3D nature of the objects (and especially the 3D facial geometry) inside the EGM architecture. That is, the proposed algorithm introduces a new structure for object representation combining both image intensity and 3D geometry information. We propose algorithms which can be used for matching robustly the object structure in novel instances. Moreover, we adopt the assumption that facial expressions are isometries of the neutral facial surface and we incorporate this inside the matching algorithm (this is based on the observation that facial skin does not stretch greatly by facial expression development).

This assumption was exploited in Bronstein et al. [6] and in [28] for creating expression invariant face Mpiperis et al. representations. In Mpiperis et al. [28] the authors provided experiments where they demonstrated that the relative change in geodesic distance is small, for facial expressions with the mouth closed.

In this paper we demonstrate the power of the proposed method in face recognition assisted by the available 3D face geometry. The proposed method in its generalized version can be applied in a fully automatic manner, combined with a face detection algorithm. The simplified version of the proposed algorithm requires the detection of the nose. The nose is the most easily detected facial feature when the 3D facial geometry is available [7,27]. On the contrary, most of the 3D face recognition algorithms proposed so far require the robust detection [16,50] of a set of facial features, which is, in general a difficult task. Furthermore, we incorporate the 3D facial geometry inside the multiscale analysis and we propose a novel Geodesic Morphological Multiscale analysis in order to fill the graph jets.

Summarizing, we propose the following advances in the EGM algorithm.

- We propose to exploit the 3D face information in the EGM procedure and moreover exploit the isometry of facial expressions in order to propose a matching procedure that is robust, to some extent, to facial expressions.
- We propose a novel geodesic morphological multiscale analysis which incorporates 3D facial geometry information inside the jets of the graph, and in that way the we create features robust to isometries of the facial surface.

- We propose a new EGM framework for face recognition based on both texture and 3D face information.

The rest of the paper is organized as follows. The 2D elastic graph matching algorithms that were proposed are briefly described in Section 2. In Section 3 we extend the matching algorithms in order to exploit the 2.5D facial models that are available from photometric stereo methods or from structure light techniques. In Section 4 we motivate an EGM architecture based on a novel multiscale geodesic morphological analysis. Experimental results are described in Section 5. Finally conclusions are drawn in Section 6.

2. 2D Elastic graph matching techniques

"One of the most popular fully automatic face recognition methods is EGM. EGM schemes consist of three steps:

- In the first step the facial image region is analyzed and a set of local descriptors is extracted at each graph node (called jets). Analysis is usually performed by building an information pyramid using scale-space techniques. In the standard EGM, a 2D Gabor-based filter bank was used for image analysis. The outputs of multiscale morphological dilation-erosion operations or the morphological signal decomposition at several scales are nonlinear alternatives of the Gabor filters for multiscale analysis. Both have been successfully used for facial image analysis [17]. Morphological feature vectors are robust to plane rotations. A jet based on Gabor filters that is robust to rotation and scaling was recently proposed in Shin et al. [33].
- In the second step a sparse graph suitable for face representation is selected. An evenly distributed rectangular graph is one of the most easy to handle automatically forms of a graph, since only a face detection algorithm is needed in order to find an initial approximation of the rectangular facial region. Other choices include graphs with nodes placed at fiducial points (like nose, mouth, eyes etc.) and the discriminant graphs proposed in Zafeiriou et al. [47], Zafeiriou and Pitas [42], and Wiskott et al. [39].
- The final step is a matching procedure of the reference graph on the test facial image in order to find the correspondences of the reference graph nodes on the test image. Simulated annealing is one of the most popular choice for solving the matching optimization procedure [47,42,33].

Formally, at each graph node, that is located at image coordinates $\mathbf{x}$, a jet (feature vector) $\mathbf{j}(\mathbf{x})$ is formed:

$$\mathbf{j}(\mathbf{x}) = [f_1(\mathbf{x}), \ldots, f_M(\mathbf{x})]^T, \tag{1}$$

where $f_i(\mathbf{x})$ denotes the output of a local operator applied to image f at the ith scale or at the ith pair (scale, orientation) and M is the jet dimensionality.

The next step of EGM is to match the reference graph on the test facial image in order to find the correspondences of the reference graph nodes on the test image. This is accomplished by minimizing a cost function that employs node jet similarities while preserving at the same time the node neighborhood relationships. Let the subscripts t and r denote a test and a reference facial image (or graph), respectively. The L_2 norm between the feature vectors at the lth graph node of the reference and the test graph is used as a similarity measure between jets. Another similarity measure that is used is the cosine between the two vectors:

$$C_f(\mathbf{j}(\mathbf{x}_t^l), \mathbf{j}(\mathbf{x}_r^l)) = \frac{\mathbf{j}(\mathbf{x}_r^l)^T \mathbf{j}(\mathbf{x}_t^l)}{\|\mathbf{j}(\mathbf{x}_r^l)\| \|\mathbf{j}(\mathbf{x}_t^l)\|}. \tag{2}$$

Let $\mathcal{V}$ be the set of all graph vertices of a certain facial image. For the rectangular graphs, all nodes, apart from the boundary nodes, have exactly four connected nodes. Let $\mathcal{N}(l)$ be the four-connected neighborhood of node l. In order to quantify the node neighborhood relationships using a measure, the relative normalized local node deformation is used:

$$C_d(\mathbf{x}_t^l, \mathbf{x}_r^l) = \sum_{\xi \in \mathcal{N}(l)} \frac{\left\| (\mathbf{x}_t^l - \mathbf{x}_t^\xi) - (\mathbf{x}_r^l - \mathbf{x}_r^\xi) \right\|}{\left\| \mathbf{x}_r^l - \mathbf{x}_r^\xi \right\|}. \tag{3}$$

In order to find the set of vertices $\left\{\mathbf{x}_t^l(r)_{\text{opt}}\right\}_{l=1}^L$ (L is fixed) out of set of all vertices $\mathcal{V}$ the following optimization problem is formulated and solved:

$$\begin{aligned} \left\{\mathbf{x}_t^l(r)_{\text{opt}}\right\}_{l=1}^L &= \min_{\{\mathbf{x}_t^l\}_{l=1}^L} C\left(\{\mathbf{x}_t^m\}_{m\in\mathcal{V}}\right) \\ &= \min_{\{\mathbf{x}_t^l\}_{l=1}^L} \sum_{m\in\mathcal{V}} \{-C_f(\mathbf{j}(\mathbf{x}_t^m), \mathbf{j}(\mathbf{x}_r^m)) + \lambda C_d(\mathbf{x}_t^m, \mathbf{x}_r^m)\}. \end{aligned} \tag{4}$$

The choice of λ in (4) controls the rigidity/plasticity of the graph [8,17].

In Kotropoulos et al. [17], the optimization of (4) was implemented as a Simulated Annealing (SA) procedure, that imposes global translation at the graph and local node deformations. In Zafeiriou and Pitas [42], in order to deal with face translation, rotation and scaling, the following optimization problem was formulated:

$$\left\{\{\boldsymbol{\delta}_l\}_{l=1}^L, \mathbf{t}, \mathbf{A}\right\}_{\text{opt}} = \min_{\{\boldsymbol{\delta}_l\}_{l=1}^L, \mathbf{t}, \mathbf{A}} C\left(\left\{\mathbf{A}\mathbf{x}_r^l + \mathbf{t} + \boldsymbol{\delta}_l\right\}\right) \tag{5}$$

The above problem can be interpreted as follows: find a wrapping matrix $\mathbf{A}$ (which in our case is a scaling and rotation matrix), a global translation $\mathbf{t}$ and a set of local node perturbations $\{\boldsymbol{\delta}_l\}_{l=1}^L$ such that the cost (4) is minimized. The optimal set of test node coordinate vectors is given by $\mathbf{x}_t^l = \mathbf{A}\mathbf{x}_r^l + \mathbf{t} + \boldsymbol{\delta}_l$. The above optimization problem is solved using SA, as well.

In Zafeiriou and Pitas [42] the above optimization problem was solved following a SA approach where random translations, scalings and rotations were tested. In order to find the local node perturbation, a local optimization problem is solved for each one of the nodes, as:

$$\begin{aligned} &\{\boldsymbol{\delta}_l\}_{\text{opt}} = \min_{\boldsymbol{\delta}_l} -C_f\left(\mathbf{j}(\mathbf{x}_r^l), \mathbf{j}\left(\mathbf{A}\mathbf{x}_r^l + \mathbf{t} + \boldsymbol{\delta}_l\right)\right) \quad \text{s.t.} \\ &C_d\left(\mathbf{x}_r^l, \mathbf{A}\mathbf{x}_r^l + \mathbf{t} + \boldsymbol{\delta}_l\right) \leqslant \tau_{\max}, \quad \text{and,} \quad \|\boldsymbol{\delta}_l\| \leqslant \delta_{\max}. \end{aligned} \tag{6}$$

where $\tau_{\max}$ and $\delta_{\max}$ are scalars that control the rigidity/plasticity of the graph.

The above algorithm can be summarized as follows:

- Initialize the algorithm using an initial guess $\left\{\mathbf{x}_t^{l\,(1)}\right\}_{l=1}^L$ (using the result of a face detector).
- For a number of steps
  - choose a global random similarity transformation (i.e., rotation, translation and scaling) in a certain range;
  - for all nodes solve the local constrained optimization problem (6);
  - check whether you accept the new solution $\left\{\mathbf{x}_t^{l\,(k)}\right\}_{l=1}^L$.
- End

2.1. A robust method using simulated annealing with a reliability criterion for nodes

Another EGM method for handling rotation and scaling using Gabor based features was proposed in Shin et al. [33]. Initially a coarse step is applied in order to find an initial graph position. Afterwards, the nodes are randomly visited in order to match them

locally. A set of reliable nodes is then selected. The reliability of the nodes is tested as follows. For each triplet of matched linked nodes (i_1,i_2,i_3) the relative angle $\theta^t(i_1,i_2,i_3)$ is calculated as:

$$\theta^t(i_1,i_2,i_3)=\cos^{-1}\left(\frac{\left(\mathbf{x}_t^{i_2}-\mathbf{x}_t^{i_1}\right)\left(\mathbf{x}_t^{i_3}-\mathbf{x}_t^{i_1}\right)}{\left\|\mathbf{x}_t^{i_2}-\mathbf{x}_t^{i_1}\right\|\left\|\mathbf{x}_t^{i_3}-\mathbf{x}_t^{i_1}\right\|}\right). \tag{7}$$

The same calculation is performed using the values of the linked nodes (i_1,i_2,i_3) of the reference graph to produce angle $\theta^r(i_1,i_2,i_3)$. Then, a test node is determined as reliable if it satisfies the following criterion:

$$|\theta^t(i_1,i_2,i_3)-\theta^r(i_1,i_2,i_3)|<\tau_\theta. \tag{8}$$

Having found this set of reliable nodes, we extract a wrapping matrix $\mathbf{A}$ and a translation vector $\mathbf{t}$ by solving a simple regression problem. The optimization problem is:

$$(\mathbf{A},\mathbf{t})_{\text{opt}}=\arg\min_{\mathbf{A},\mathbf{t}}\sum_{k\in\mathcal{L}}\|\mathbf{x}_t^k-(\mathbf{A}\mathbf{x}_r^k+\mathbf{t})\|^2 \tag{9}$$

where $\mathcal{L}$ is the set of reliable nodes and $\mathbf{t}$ represents the translational vector between graphs. For a set of six parameters, at least 3 reliable nodes should be identified. A simple regression is sufficient for finding matrix $\mathbf{A}$ and vector $\mathbf{t}$. We used the regressor available in Press et al. [30].

After solving (9), the optimal wrapping matrix $\mathbf{A}_{\text{opt}}$ and translation vector $\mathbf{t}_{\text{opt}}$ are applied to all nodes and the whole procedure is repeated. A series of steps, including scaling, rotation, translation and local node perturbations are then calculated. The algorithm is summarized as follows.

- Initialize the algorithm using a coarse matching procedure $\left\{\mathbf{x}_t^{l^{(1)}}\right\}_{l=1}^{L}$.
- For a number of steps
  - for all nodes solve the local optimization problem (6);
  - if the reliable nodes (reliable according to (8)) are more than 3, then estimate the wrapping matrix $\mathbf{A}_{\text{opt}}$ and the translation vector $\mathbf{t}_{\text{opt}}$;
  - re-estimate the position of all nodes according to the wrapping matrix $\mathbf{A}_{\text{opt}}$ and the translation vector $\mathbf{t}_{\text{opt}}$.
- If $\left|\sum_{l\in\mathcal{V}}\left\{C_f\left(\mathbf{j}\left(\mathbf{x}_t^{l^{(k)}}\right),\mathbf{j}(\mathbf{x}_r^l)\right)\right\}-\sum_{l\in\mathcal{V}}\left\{C_f\left(\mathbf{j}\left(\mathbf{x}_t^{l^{(k-1)}}\right),\mathbf{j}(\mathbf{x}_r^l)\right)\right\}\right|<\epsilon$, then stop.

In Shin et al. [33] the nodes were visited randomly and were locally optimized based on a SA strategy. Finally, the SA was cooled after the re-initialization of all nodes. The final measure $\sum_{l\in\mathcal{V}}\{-C_f(\mathbf{j}(\mathbf{x}_t^l),\mathbf{j}(\mathbf{x}_r^l))\}$ was used for quantifying the distance between the reference graph and the test image.

3. 2.5D matching algorithm

In this Section we describe the proposed matching algorithm which makes use of the available 2.5D facial information. The geodesic distances between the points can be calculated given the facial surface. Moreover, they are robust against isometry mappings (or isometries) of the facial surface. The facial pose variations are isometries of the facial surfaces. Up to a certain extent, facial expressions can be safely regarded as isometries, as well, as long as the mouth remains closed. That is, the geodesic distances before and after the development of an expression are considered to remain (approximately) the same. Recently, a lot of research was conducted in order to create expression invariant representations for face recognition [6,28], where facial expressions were modelled as isometries of the facial surface. The notion of geodesic distance, the geodesic path and the angle between geodesic paths are pictorially described in Fig. 1. Fig. 1a depicts the geodesic distance d and polar angle θ of a point $\mathbf{Q}$ on the surface. Geodesic path g between two points $\mathbf{P}$ and $\mathbf{Q}$ of the surface is the minimum length curve connecting the two points. Geodesic distance d is the length of path g. The geodesic angle θ is the angle between the tangents of the geodesic path g and the reference geodesic path g_0 at point $\mathbf{P}$. In Fig. 1b the 2.5D facial surface and the corresponding graph are depicted. The simplified facial grid with simple connections is depicted in Fig. 1c. The geodesic grid with the connections between nodes being the geodesic path between nodes is depicted in Fig. 1d.

By incorporating the isometry assumption in the EGM architecture, a matching procedure is implemented in which the nodes can be deformed in such a way that the geodesic distances are approximately preserved during the matching procedure. In our case, the 2.5D information was derived from photometric stereo [2] and the integration of the normal field [11]. Thus a height map $g(\mathbf{x})\in\Re$ was acquired for every pixel of the image as $\mathbf{x}\in\mathcal{Z}^2$. Let $\mathcal{X}_g$ be a set of connections between the points of the surface which defines the topology of the surface. The set of connections is derived from a dense triangulation of the image domain (in our implementation we used a simple Delauney triangulation). Let that $\mathcal{G}=(g,\mathcal{X}_g)$ denote the tuple that contains both the depth map and the topology of the facial surface. The triangulated surface is only needed to compute the geodesics. In other words, we have a 2D graph but in order to compute the distances between the graph nodes we use the triangulated surface.

Optimization problem (4) in now modified, using the same rectangular sparse graph, in such a way as to find a set of vertices $\{\mathbf{x}_t^l(r),l\in\mathcal{V}\}$ in the test image that minimizes cost function

$$C_{\mathcal{G}}(\{\mathbf{x}_t^l\})=\sum_{l\in\mathcal{V}}\left(-\{C_f(\mathbf{j}(\mathbf{x}_t^l),\mathbf{j}(\mathbf{x}_r^l)+\lambda\sum_{\xi\in\mathcal{N}(l)}\left(\frac{|d_{\mathcal{G}}(\mathbf{x}_t^l,\mathbf{x}_t^\xi)-d_{\mathcal{G}}(\mathbf{x}_r^l,\mathbf{x}_r^\xi)|}{d_{\mathcal{G}}(\mathbf{x}_r^l,\mathbf{x}_r^\xi)}\right)\right) \tag{10}$$

where $d_{\mathcal{G}}(\mathbf{x}_1,\mathbf{x}_2)$ is the geodesic distance between points $\mathbf{x}_1$ and $\mathbf{x}_2$ of the triangulated surface $\mathcal{G}$.

The corresponding local optimization problem (6) we have to solve in order to estimate the local perturbation is now formulated as:

$$\begin{aligned}&\{\boldsymbol{\delta}_l\}_{\text{opt}}=\min_{\boldsymbol{\delta}_l}-C_f^2\left(\mathbf{j}(\mathbf{x}_r^l),\mathbf{j}\left(\mathbf{A}\mathbf{x}_r^l+\mathbf{t}+\boldsymbol{\delta}_l\right)\right)\text{s.t.}\\&d_{\mathcal{G}}\left(\mathbf{x}_r^l,\mathbf{A}\mathbf{x}_r^l+\mathbf{t}+\boldsymbol{\delta}_l\right)\leqslant\tau,\text{and},\|\boldsymbol{\delta}_l\|\leqslant\delta_{\max}.\end{aligned} \tag{11}$$

The local optimization problem is schematically described in Fig. 2.

The proposed EGM algorithm that uses the available 3D facial geometry is as follows. First, a coarse step is applied and a first approximation of the graph is calculated. The coarse step can be a simple implementation of the step described in the previous Section. For every node a constrained local search is performed in order to solve (11). Moreover, instead of using $\mathbf{x}$, $\mathbf{z}(\mathbf{x})$ can be used so as to find a 3×3 wrapping matrix $\mathbf{A}$. In this case at least three reliable nodes should be identified. After all nodes were visited, the set of reliable nodes is extracted. In our case, since 2.5D information is available and in order to retain robustness against pose variations, criterion (8) is generalized as follows. Let i_1,i_2,i_3 be three linked nodes. The relative angle around a matched node (similar to (7)) is calculated as:

$$\theta^t(i_1,i_2,i_3)=\theta_{\mathcal{G}}(i_1,i_2,i_3) \tag{12}$$

where $\theta_{\mathcal{G}}$ is the angle between the geodesic path i_1,i_2 and the geodesic path i_1,i_3 (as shown in Fig. 3) and superscript t refers to the test image. All angles are robust against out of plane facial pose changes. Examples of the relative geodesic and grid angles are depicted in Fig. 3a and b.

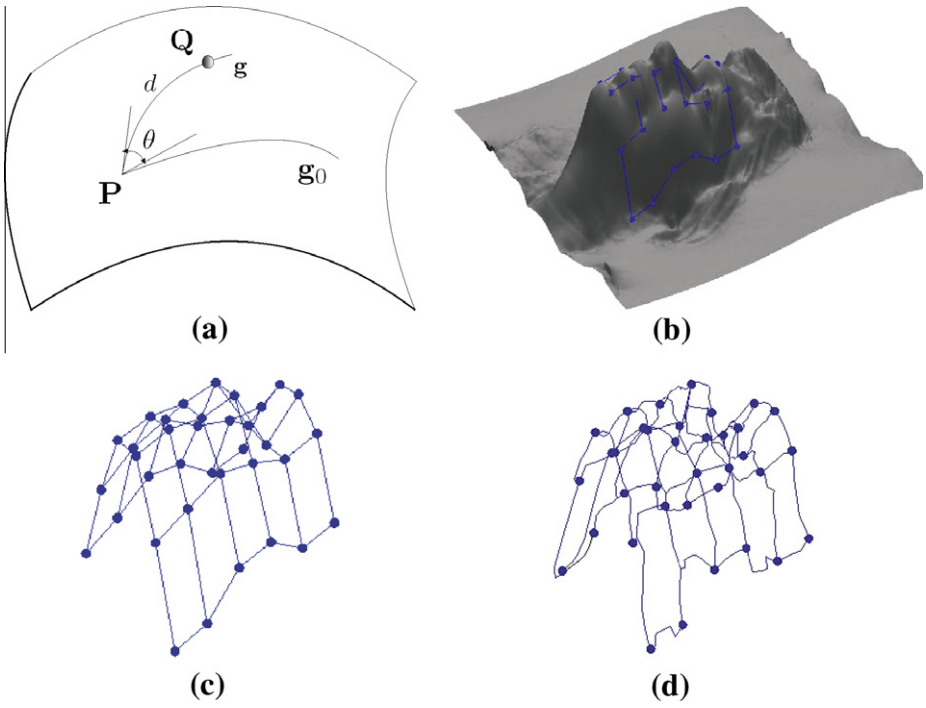

Fig. 1. (a) Geodesic paths and geodesic angles; (b) the facial geometry and the graph; (c) the 3D grid; (d) the 3D geodesic graph.

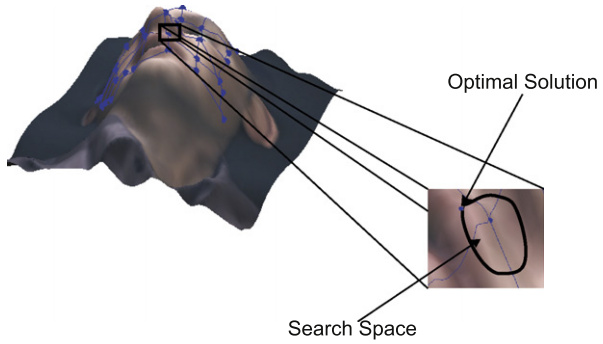

Fig. 2. Local optimization problem (11).

If we consider that the neighborhood of $\mathcal{N}(l)$ is sufficiently local[1] (i.e., we have a dense graph and a topology without holes) then we may approximate

$$d_{\mathcal{G}}(\mathbf{x}_1,\mathbf{x}_2) \approx \|\mathbf{z}(\mathbf{x}_1)-\mathbf{z}(\mathbf{x}_2)\| \tag{13}$$

where $\mathbf{z}(\mathbf{x}) = [\mathbf{x}g(\mathbf{x})]^T$. Subsequently we may approximate :

$$\theta(i_1,i_2,i_3)^t \approx \cos^{-1}\left(\frac{\left(\mathbf{z}\left(\mathbf{x}_t^{i_3}\right)-\mathbf{z}\left(\mathbf{x}_t^{i_1}\right)\right)\left(\mathbf{z}\left(\mathbf{x}_t^{i_2}\right)-\mathbf{z}\left(\mathbf{x}_t^{i_1}\right)\right)}{\left\|\mathbf{z}\left(\mathbf{x}_t^{i_3}\right)-\mathbf{z}\left(\mathbf{x}_t^{i_1}\right)\right\|\left\|\mathbf{z}\left(\mathbf{x}_t^{i_2}\right)-\mathbf{z}\left(\mathbf{x}_t^{i_1}\right)\right\|}\right). \tag{14}$$

After the set of reliable nodes is found, a 3×3 wrapping matrix is calculated by solving a similar optimization as (9). Afterwards, this wrapping matrix is used for recalculating all node positions. The whole procedure is repeated in a similar way as the algorithm in the previous Section. A matching result is shown in Fig. 4a and b.

In order to simplify the procedure, we shall introduce a modification of the generalized algorithm proposed above. Assume that only certain facial features, like the nose, are available. The nose is one of the most easily detected features upon the facial surface [7,27]. Given the position of the nose (points $\mathbf{x}_{\text{nose}}{}^{l}$ and $\mathbf{x}_{\text{nose}}{}^{t}$) an initial estimation for the position of the graph is provided so that we can search for small translations. An example of the nose tip and the geodesic path of every node and the nose tip is shown in Fig. 5. Afterwards, under the assumption that facial expressions are isometries on the facial surface, we confine our local search, in the local matching procedure, to areas in which the geodesic distance between the position of the reference node and the position of the test node does not significantly change. Given the position of the node we can modify the local search problem as:

$$\begin{aligned}&\min_{\delta_l}\left\{-C_f\left(\mathbf{j}(\mathbf{x}_r^l+\boldsymbol{\delta}_l),\mathbf{j}(\mathbf{x}_r^l)\right)\right\}\text{subject to}\\&\left|\frac{d_{\mathcal{G}}(\mathbf{x}_r^l,\mathbf{x}_{\text{nose}}^l)-d_{\mathcal{G}}(\mathbf{x}_r^l+\boldsymbol{\delta}_l,\mathbf{x}_{\text{nose}}^t)}{d_{\mathcal{G}}(\mathbf{x}_r^l,\mathbf{x}_{\text{nose}}^l)}\right|\leqslant\tau_1,\ \|\boldsymbol{\delta}_l\|\leqslant\delta_{\max}.\end{aligned} \tag{15}$$

The new local search is pictorially described in Fig. 6.

4. Geodesic multiscale morphological elastic graph matching

In the previous Section we described a method that incorporates the available 2.5D information in the matching procedure in order to obtain a pose invariant matching. Moreover, the matching is to some extend invariant to facial expressions, as well. In this Section, we present features that are robust against facial pose variations and facial expressions. To that end we describe a Multiscale Morphological Analysis (MMA) that is robust against pose variations, the so-called Geodesic MMA (GMMA). Moreover, under the isometry assumption (i.e, preservation of geodesic distances) the proposed MMA analysis can be to some extent robust under facial expression development.

[1] Sufficiently that the actual geodesic distance between two neighboring nodes of the graph is approximately the euclidean distance as given by Eq. (11). This depends on the resolution of the facial image. Preliminary experiments with images where facial region is of resolution about 100×100 graph nodes placed at every four or five pixels indicated that the euclidean distance provides a good approximation. This approximation is valid in dense graphs. In all conducted experiments in this paper we used the actual geodesic distance and not the approximation.

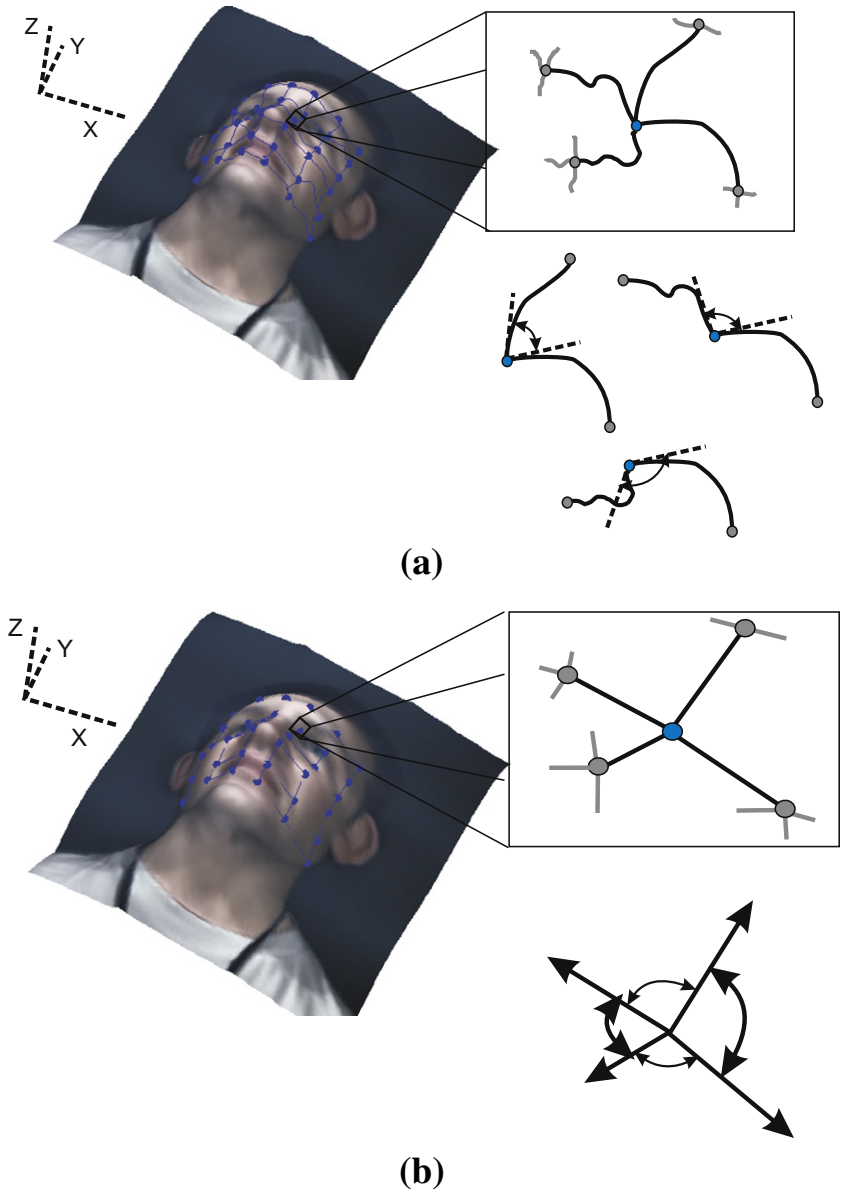

Fig. 3. (a) Relative geodesic angles in (12); (b) relative angles in case (14).

MMA for facial image analysis was initially proposed in Kotropoulos et al. [17] and was well incorporated in a Morphological EGM (MEGM) architecture. Another modified MEGM was presented in Zafeiriou et al. [46]. In MEGM an information pyramid is built using multiscale morphological dilations-erosions. Given an image $f(\mathbf{x}) : \mathcal{D} \subseteq \mathcal{Z}^2 \rightarrow \Re$ where $\mathcal{D}$ is the support of the original image and a structuring function $h_\sigma(\mathbf{x}) : \mathcal{H}_\sigma \subseteq \mathcal{Z}^2 \rightarrow \Re$ where $\mathcal{H}_\sigma$ is the image support of the structuring element with scale σ, the dilation of the image $f(\mathbf{x})$ by $h_\sigma(\mathbf{x})$ is denoted by $(f \oplus h_\sigma)(\mathbf{x})$. Its complementary operation, the erosion, is denoted by $(f \ominus h_\sigma)(\mathbf{x})$ [17]. The multiscale dilation-erosion pyramid of the image $f(\mathbf{x})$ by $h_\sigma(\mathbf{x})$ is defined as

$$(f * h_\sigma)(\mathbf{x}) = \begin{cases} (f \oplus h_\sigma)(\mathbf{x}) & \text{if } \sigma > 0 \\ f(\mathbf{x}) & \text{if } \sigma = 0 \\ (f \ominus h_{|\sigma|})(\mathbf{x}) & \text{if } \sigma < 0 \end{cases} \tag{16}$$

where σ denotes the scale parameter of the structuring function. In Kotropoulos et al. [17] it was shown that the choice of the structuring function does not lead to statistically significant changes in the verification performance. However, it affects the computational complexity of feature calculation. The efficient computation of dilations and erosions is a factor of great importance in practical applications.

In this paper we use, for simplicity of computations, only flat structuring elements (i.e., $h_\sigma(\mathbf{v}) = 0, \forall \mathbf{v} \in \mathcal{H}_\sigma, \|\mathbf{v}\| \leqslant |\sigma|$). For this type of structuring elements, the dilation and the erosion can be written as:

$$\begin{aligned} (f \oplus h_\sigma)(\mathbf{x}) &= \sup_{\mathbf{y} \in \mathcal{H}_\sigma} f(\mathbf{x} - \mathbf{y}) \\ (f \ominus h_{|\sigma|})(\mathbf{x}) &= \inf_{\mathbf{y} \in \mathcal{H}_\sigma} f(\mathbf{x} - \mathbf{y}) \end{aligned} \tag{17}$$

For a flat structuring function, dilations can be efficiently computed by applying running min/max calculations in which the computation of one scale exploits the previous outcome. That is, scale-recursive computations that speed up considerably feature calculation can be used. For a flat structuring function, scale-recursive max computations (i.e., multiscale image dilations) are based on the observation that:

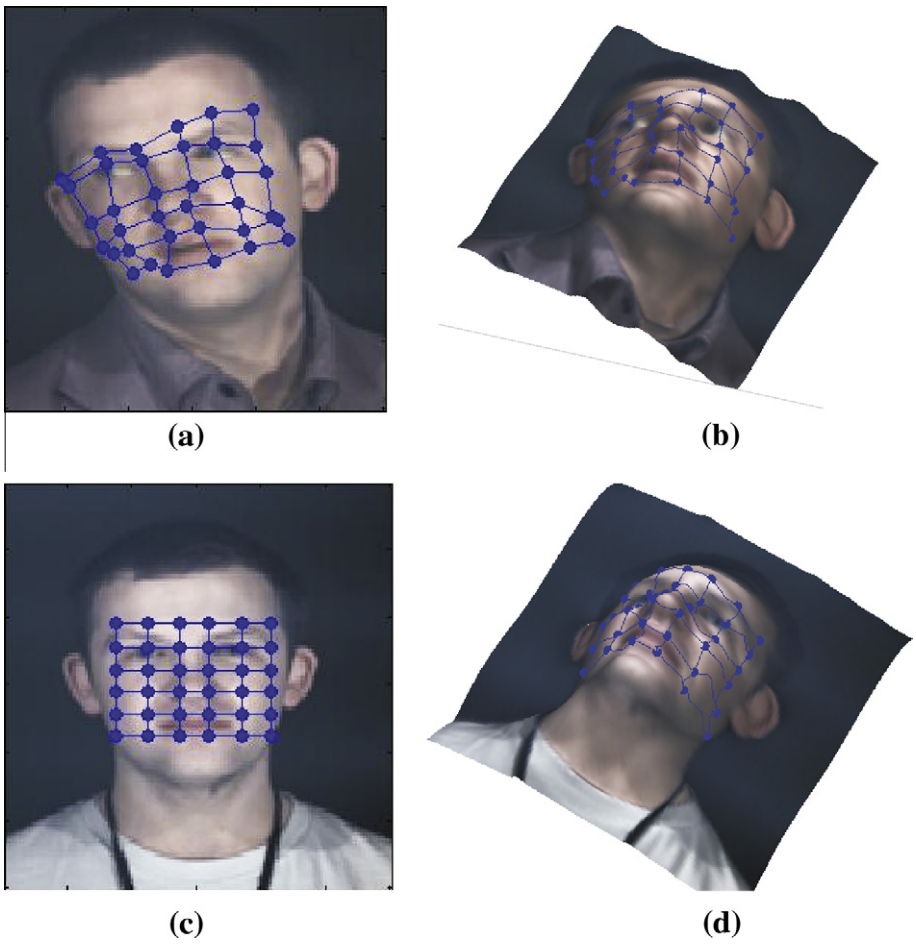

Fig. 4. (a) The 2D reference graph; (b) the facial geometry and the graph; (c) the matched graph on a test image; (d) the facial geometry and the resultant graph.

Fig. 5. A graph that is built around the nose.

$$(f \oplus h_\sigma)(\mathbf{x}) = \max\{(f \oplus h_\sigma)(\mathbf{x}), \max_{\mathbf{y}\in\Delta\mathcal{H}(\sigma+1)}\{f(\mathbf{x}+\mathbf{y})\}, \max\{f(\mathbf{x}\pm\mathbf{s})\}\} \tag{18}$$

where $\mathbf{s} = [\sigma+1\ \sigma+1]^T$, set $\Delta\mathcal{H}(\sigma_{i+1}) = \{\mathbf{y} = [y_1 y_2]^T \in \mathcal{Z}^2 : \|\mathbf{y}\|^2 > \sigma^2, \|\mathbf{y}\|^2 \leqslant (\sigma+1)^2, |y_1| \leqslant \sigma, |y_2| \leqslant \sigma\}$. A similar multiscale analysis can be applied for the calculation of the erosion. In order to use the available 2.5D information we define the surface depended structuring flat elements around $\mathbf{x}$ as:

$$g_{\sigma\mathbf{x}}(\mathbf{v}) = 0, \forall \mathbf{v} \in \{\mathbf{y} \in \mathcal{Z}^2 : d_{\mathcal{G}}(\mathbf{v},\mathbf{x}) \leqslant |\sigma|\} \tag{19}$$

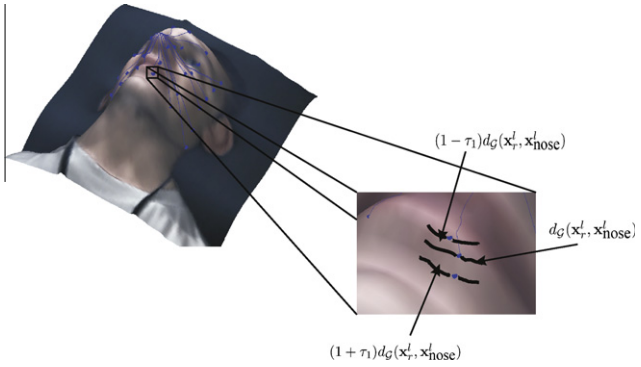

Fig. 6. Local optimization problem (15).

The above equation defines a flat structuring element upon a geodesic circle of scale σ.

The new multiscale morphological analysis, given a height map g with a topology $\mathcal{X}_g$, as follows:

$$(f \oplus g_{\sigma_i})_{\mathcal{G}}(\mathbf{x}) = \max\{(f \oplus g_{\sigma_{i-1}})_{\mathcal{G}}(\mathbf{x}), \max_{(\mathbf{v}\in\Delta\mathcal{H}_{\mathcal{G}}(\mathbf{x},\sigma_i)}\{f(\mathbf{v})\}\}. \tag{20}$$

Here $\Delta\mathcal{H}_{\mathcal{G}}(\mathbf{v},\sigma_i) = \{\mathbf{y} \in \mathcal{Z}^2 : \sigma_{i-1} < d_{\mathcal{G}}(\mathbf{v},\mathbf{y}) \leqslant \sigma_i\}$. In the same manner, we have for the erosions:

$$(f \ominus g_{|\sigma_i|})_{\mathcal{G}}(\mathbf{x}) = \min\{(f \ominus g_{\sigma_{i-1}})_{\mathcal{G}}(\mathbf{x}), \min_{(\mathbf{v}\in\Delta\mathcal{H}_{\mathcal{G}}(\mathbf{x},\sigma_i)}\{f(\mathbf{v})\}\}. \tag{21}$$

In order to have a scale invariant GMMA we can modify the above as follows: $\Delta\mathcal{H}_{\mathcal{G}}(\mathbf{v},\sigma_i)=\{\mathbf{y}\in\mathcal{Z}^2:(i-1)\sigma_1<d_{\mathcal{G}}(\mathbf{v},\mathbf{y})\leqslant i\sigma_1\}$ where $\sigma_1=\mu\max\{d_{\mathcal{G}}(\mathbf{x}_{\text{nose}},\mathbf{x})\}$. $\max\{d_{\mathcal{G}}(\mathbf{x}_{\text{nose}},\mathbf{x})\}$ is the maximum geodesic distance between the nose and the given facial surface. In this paper we set $\mu=1/(\max\{R_1,R_2\})$ where R_1 and R_2 are the number of image rows and columns, respectively. Examples of geodesic circles are given in Fig. 7. The maximum geodesic distance of nose in the given facial surface normalized by the number of rows or columns is a measure robust to scale variations in 2.5D images and provides us the first scale of the multiscale analysis. This normalization step is conducted in order to have a scale insensitive estimation σ_1.

The problem now becomes that of the efficient computation of GMFA. For the first scale, for all $\mathbf{x}$ we have to compute the geodesic circle of radius σ_1, i.e. $\mathcal{H}_{\sigma_1}(\mathbf{x})=\{\mathbf{y}\in\mathcal{Z}^2:d_{\mathcal{G}}(\mathbf{x},\mathbf{y})\leqslant\sigma_1\}$.

The calculation of $\mathcal{H}_{\sigma_2}(\mathbf{x})$ for the next scale can be performed by exploiting the property that if $\mathbf{y}\in\mathcal{H}_{\sigma_1}(\mathbf{x})$ then $\mathbf{x}\in\mathcal{H}_{\sigma_1}(\mathbf{y})$. This leads to $\sigma_2=2\sigma$:

$$\begin{aligned}&\mathcal{H}_{2\sigma}(\mathbf{x})=\bigcup_{\mathbf{y}\in\mathcal{H}_{\sigma}(\mathbf{x})}\mathcal{H}_{\sigma}(\mathbf{y})\\&\Delta\mathcal{H}_{\mathcal{G}}(\mathbf{x},2\sigma)=\mathcal{H}_{2\sigma}(\mathbf{x})-\mathcal{H}_{\sigma}(\mathbf{x}).\end{aligned}\tag{22}$$

In the general case, we have:

$$\begin{aligned}&\mathcal{H}_{\sigma_i}(\mathbf{x})=\bigcup_{\mathbf{y}\in\mathcal{H}_{\sigma_{i-1}}(\mathbf{x})}\mathcal{H}_{\sigma_{i-1}}(\mathbf{y})\\&\Delta\mathcal{H}_{\mathcal{G}}(\mathbf{x},\sigma_i)=\mathcal{H}_{\sigma_i}(\mathbf{x})-\mathcal{H}_{\sigma_{i-1}}(\mathbf{x})\end{aligned}\tag{23}$$

Thus, we only have to find a look-up table for the first scale and the next scales can be computed in a scale recursive strategy by using (23).

We can therefore build the GMMA $(f\bigstar h_\sigma)_{\mathcal{G}}(\mathbf{x})$ in a similar manner as (16) using dilation defined by (20) and erosion by (21) as

$$(f\bigstar g_\sigma)_{\mathcal{G}}(\mathbf{x})=\begin{cases}(f\oplus g_\sigma)_{\mathcal{G}}(\mathbf{x}) & \text{if } \sigma>0\\ f(\mathbf{x}) & \text{if } \sigma=0\\ (f\ominus g_\sigma)_{\mathcal{G}}(\mathbf{x}) & \text{if } \sigma<0\end{cases}\tag{24}$$

The output of these morphological operations forms the jet $\mathbf{j}(\mathbf{x}^l)$, at graph node l, that is located at image coordinates $\mathbf{x}^l$:

$$\begin{aligned}\mathbf{j}(\mathbf{x}^l)=&((f\bigstar h_{\sigma_\Lambda})_{\mathcal{G}}(\mathbf{x}^l),\ldots,(f\bigstar h_{\sigma_1})_{\mathcal{G}}(\mathbf{x}^l),f(\mathbf{x}^l),\\&(f\bigstar h_{\sigma_{-1}})_{\mathcal{G}}(\mathbf{x}^l),\ldots,(f\bigstar h_{\sigma_{-\Lambda}})_{\mathcal{G}}(\mathbf{x}^l))\end{aligned}\tag{25}$$

where Λ is the number of different scales used. An example of the typical multiscale morphological operations proposed in Kotropoulos et al. [17] for a flat structuring element is shown in Fig. 8 a. The geodesic multiscale morphological analysis is shown in Fig. 8 b.

5. Experimental results

In this Section, we conducted experiments in order to assess how the proposed advances improve the performance of EGM algorithms in case that 2.5D object information is available. We present experiments for face recognition/verification using photometric stereo. The experiments are the first reported for such a large face database that use photometric stereo. Before we describe the experiments, we shall briefly describe how we have set up our hardware for the high speed imaging and light source sequencing necessary for facial photometric stereo. Our system has been designed for practical 3D face geometry capture and recognition. Individuals walk through the archway towards the camera located on the back panel and exit through the side. This arrangement

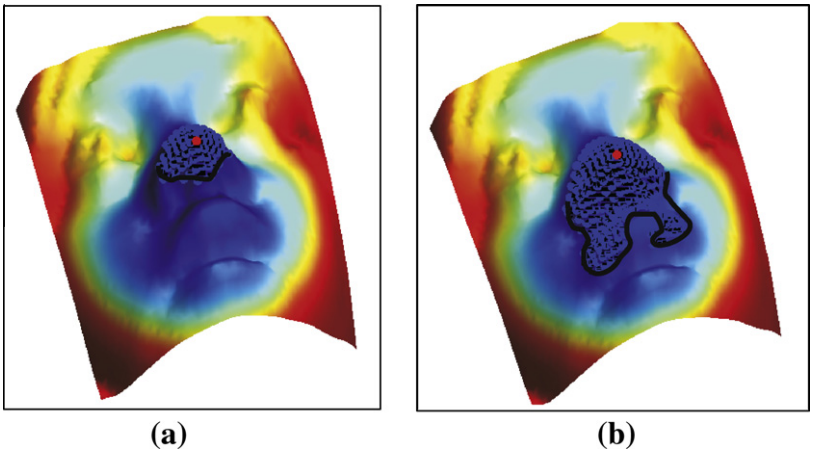

Fig. 7. (a) Geodesic circle of $2\sigma_1$; (b) geodesic circle of $5\sigma_1$.

Fig. 8. The upper left image is the original image extracted is both figures. The first nine images starting from the left corner, apart from the upper left one, are the eroded images and the remaining nine are the dilated images (a) for multiscale dilations-erosions for nine scales; (b) geodesic multiscale dilations-erosions.

makes the device suitable for use at the entrance to buildings, high security areas, airports etc. The presence of an individual is detected by an ultrasound proximity sensor placed before the archway.

The sensor triggers the sequence of high speed synchronised frame grabbing and light source switching. We found experimentally that for people casually passing through the device, a minimum frame rate of approximately 150 fps was necessary to avoid significant movement between frames. Our device currently operates at 200 fps. For the light sources we have used four Jessops M100 flashguns. A monitor is included on the back panel to indicate whether the face has been recognised/authorised or to display other information. For each person passing through the device, the following sequence of events takes place to capture the four images: (1) Await signal from ultrasound sensor, (2) send trigger to camera (3) await integration-enabled signal from camera, (4) discharge flashgun, (5) await end of integration enabled signal, (6) repeat from step 2 for the remaining light sources. All interfacing code is written in NI LabVIEW.

We now show some results of using our image capture device for facial geometry reconstruction. Fig. 9 shows an example of four raw images of an individual. The person was slowly (1 m/s), but casually, walking through the device. A database of faces was collected setting a device for proper capture of four images under four different lighting directions. This is the first large photometric stereo face database that is collected and we are now trying to make it publicly available. The four intensity images were processed using a standard photometric stereo method [1]. This resulted in a dense field of surface normals, which we integrated to form height maps using the well-known Frankot and Chellappa method [11]. The corresponding albedo and height map are depicted in Fig. 10.

The device was installed in the premises of General Dynamics. Staff and visitors were invited to use it. After a period of more than 6 months more than 250 persons were recorded. 98 walked through the device only once. For 113 out of the remaining 152 persons who walked though the device more than once we collected images taken with more than a week's interval and for the remaining 39 we collected samples with not more than 3 days interval. For the majority of 113 individuals (about 90 people) the interval was greater than one month. We decided to use as clients only those for which the training and the testing sample was collected at least after one week. The remaining individuals served as impostors.

For the experiments presented here, a very challenging experimental procedure was followed, using only one grayscale albedo image and the triangulated height map in order to create the reference graph, and one grayscale albedo image and a triangulated height map for testing. Most of the training and testing images display a different facial expression and have a slightly different pose. An example of training and testing images can be found in Fig. 4. One-sample face recognition is among the most challenging face recognition scenarios with a lot of applications. In Rizvi et al. [31] a face verification scenario was designed based only on one sample per person for training. The interested reader could refer to Tan et al. [34] and in the references therein for more details about one sample face recognition.

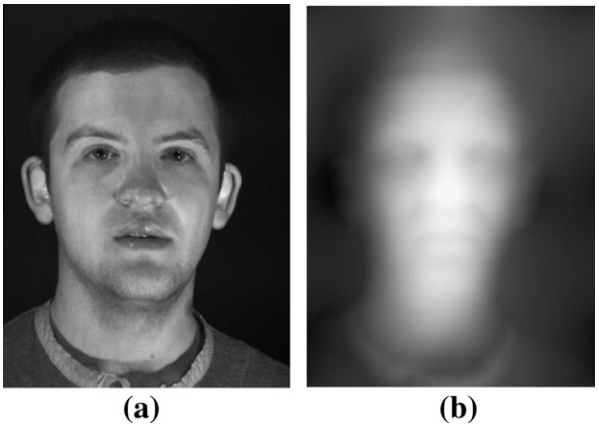

Fig. 10. (a) The grayscale albedo image; (b) the depth map image.

For comparisons, apart from the tested EGM approaches, we have implemented other methods that can be used using only one sample. Such techniques include Principal Component Analysis (PCA) [37] and Nonnegative Matrix Factorization [22,41,43]. For the above tested methods and for a fair comparison, the albedo and depth map images were aligned manually, using the eye coordinates, and were downsampled to 90×100. On the other hand all the tested EGM algorithms were combined with a face detector (the face detection module of OpenCV [5]) in fully automatic

Table 1
The rank-1 recognition results of the tested methods.

PCA	NMF	MEGM	2.5D-MEGM	GMEGM
42%	63%	78%	82%	87%

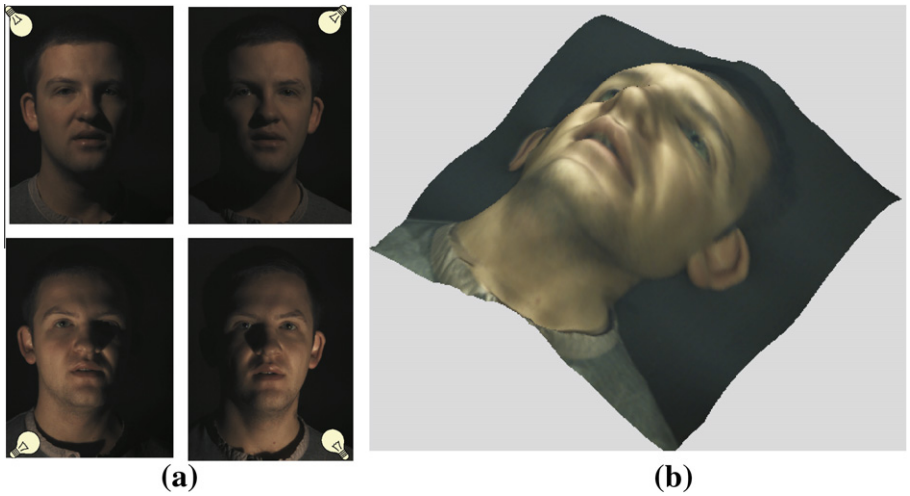

Fig. 9. (a) Four images taken for four different lighting directions; (b) the corresponding 2.5D model.

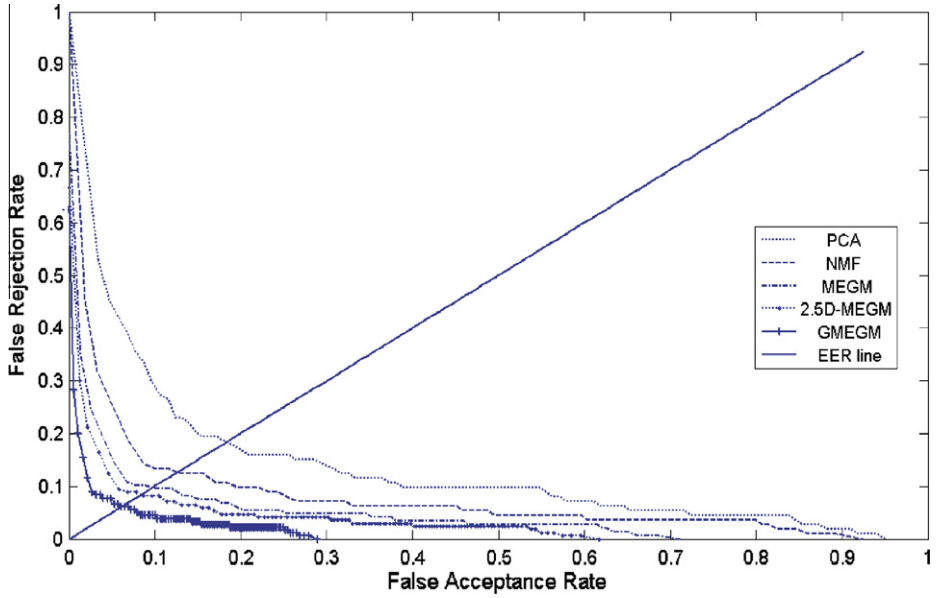

Fig. 11. ROC curves for the tested methods.

Table 2
The EER of the tested methods.

PCA	NMF	MEGM	2.5D-MEGM	GMEGM
18.4%	12.6%	10%	8.4%	6%

manner. For the EGM algorithms we use the abbreviation 2.5D-MEGM for MEGM using the 2.5D matching procedure presented in Section 3. The abbreviation GMEGM stands for the geodesic elastic graph matching with the 2.5D matching procedure presented in Section 4. The recognition rates for the tested methods are summarized in Table 1.

Verification experiments were conducted in the same database as well. The verification protocol was similar to the one defined in the FERET verification protocol in Rizvi et al. [31]. The probe (or client set) was defined by the 113 persons. The first image is used for training while the second is used for testing client claims. The remaining 140 persons of the database, with one image per person, are considered the impostors. In other words, in the test phase we have only one image for measuring the false rejection (FR) rates and one image per person remaining in the database is used for measuring the false acceptance (FA) rates. The Receiver Operation Characteristics (ROC) curves are summarized in Fig. 11. The performance of the algorithms is quoted for the Equal Error Rate (EER) which is the scalar figure of merit that is often used to judge the performance of a verification algorithm. The EER of the tested methods is summarized in Table 2.

As it can be seen, the proposed methods greatly advances the performance of EGM for face recognition/verification.

6. Conclusions

In this paper a two advances in the EGM algorithm were proposed in order to capitalize on the available 2.5D facial information using modern techniques. We modified the matching technique in order to exploit the facial geometry information. The proposed matching procedure is robust against pose changes and also takes into consideration changes of the facial surfaces under facial expressions. We incorporated the 2.5D information in a multiscale morphological analysis and built that way a geodesic multiscale morphological analysis which is robust against facial pose changes. The first large scale experimental results for face recognition/verification using photometric stereo show that the proposed approach advances the performance of EGM.

Acknowledgment

This work was supported by the EPSRC project EP/E028659/1 Face Recognition using Photometric Stereo.

References

[1] V. Argyriou, M. Petrou, Photometric stereo: an overview, Advances in Imaging and Electronic Physics 156 (2008) 1–55.
[2] S. Barsky, M. Petrou, The 4-source photometric stereo technique for three-dimensional surfaces in the presence of highlights and shadows, IEEE Transactions on Pattern Analysis and Machine Intelligence (25) (2003) 1239–1252.
[3] S. Barsky, M. Petrou, Design issues for a colour photometric stereo system, Journal of Mathematical Imaging and Vision (24) (2006) 143–162.
[4] K. Bowyer, K. Chang, P. Flynn, A survey of approaches and challenges in 3d and multi-modal 3d + 2d face recognition, Computer Vision and Image Understanding 101 (1) (2006) 1–15.
[5] G. Bradski, A. Kaehler, Learning OpenCV: Computer Vision with the OpenCV Library, 2008.
[6] A. Bronstein, M. Bronstein, R. Kimmel, Expression-invariant representations of faces, IEEE Transactions on Image Processing 16 (1) (2007) 188–197.
[7] K. Chang, K. Bowyer, P. Flynn, Multiple nose region matching for 3D face recognition under varying facial expression, IEEE Transactions on Pattern Analysis and Machine Intelligence 28 (10) (2006) 1695–1700.
[8] B. Duc, S. Fischer, J. Bigün, Face authentication with Gabor information on deformable graphs, IEEE Transactions on Image Processing 8 (4) (1999) 504–516.
[9] C. Eckes, J. Triesch, C.v.d. Malsburg, Analysis of cluttered scenes using and elastic matching approach for stereo images, Neural Computation 18 (2006) 1441–1471.
[10] P. Flynn, T. Faltemier, K.W. Bowyer, 3d face recognition, in: A.K. Jain, A. Ross, P.J. Flynn (Eds.), Handbook of Biometrics, Springer, 2008, pp. 211–229.
[11] R. Frankot, R. Chellappa, A method for enforcing integrability in shape from shading algorithms, IEEE Transactions on Pattern Analysis and Machine Intelligence 10 (4) (1988) 439–451.
[12] D. Gonzalez-Jimenez, J. Alba-Castro, Shape-driven Gabor jets for face description and authentication, IEEE Transactions on Information Forensics and Security 2 (4) (2007) 769–780.
[13] G.-D. Guo, C.R. Dyer, Learning from examples in the small sample case: face expression recognition, IEEE Transactions Systems, Man, and Cybernetics, Part B: Cybernetics 35 (3) (2005) 479–488.
[14] H. Hong, H. Neven, C.v.d. Malsburg, Online facial expression recognition based on personalized gallery, in: Intl. Conference on Automatic Face and Gesture Recognition. Nara, Japan, 14–16, 1998, pp. 354–359.

[15] D.G. Jimenez, J.L.A.C. Castro, Shape contexts and Gabor features for face description and authentication, in: IEEE International Conference on Image Processing (ICIP 2005), Genova, 11–14 September 2005.
[16] I. Kakadiaris, G. Passalis, G. Toderici, M.N. Murtuza, Y. Lu, N. Karampatziakis, T. Theoharis, Three-dimensional face recognition in the presence of facial expressions: an annotated deformable model approach, IEEE Transactions on Pattern Analysis and Machine Intelligence 29 (4) (2007) 640.
[17] C. Kotropoulos, A. Tefas, I. Pitas, Frontal face authentication using discriminating grids with morphological feature vectors, IEEE Transactions on Multimedia 2 (1) (2000) 14–26.
[18] C. Kotropoulos, A. Tefas, I. Pitas, Frontal face authentication using morphological elastic graph matching, IEEE Transactions on Image Processing 9 (4) (2000) 555–560.
[19] C. Kotropoulos, A. Tefas, I. Pitas, Morphological elastic graph matching applied to frontal face authentication under well-controlled and real conditions, Pattern Recognition 33 (12) (2000) 31–43.
[20] N. Krüger, An algorithm for the learning of weights in discrimination functions using a priori constraints, IEEE Transactions on Pattern Analysis and Machine Intelligence 19 (7) (1997) 764–768.
[21] M. Lades, J.C. Vorbrüggen, J. Buhmann, J. Lange, C.v.d. Malsburg, R.P. Würtz, W. Konen, Distortion invariant object recognition in the dynamic link architecture, IEEE Transactions on Computers 42 (3) (1993) 300–311.
[22] D. Lee, H. Seung, Algorithms for non-negative matrix factorization, in: NIPS, 2000, pp. 556–562. <citeseer.ist.psu.edu/lee01algorithms.html>.
[23] M. Lyons, S. Akamatsu, M. Kamachi, J. Gyoba, Coding facial expressions with Gabor wavelets, in: Intl. Conference on Automatic Face and Gesture Recognition. Nara, Japan, 14–16 1998, pp. 200–205.
[24] M. Lyons, J. Budynek, S. Akamatsu, Automatic classification of single facial images, IEEE Transactions on Pattern Analysis and Machine Intelligence 21 (12) (1999) 1357–1362.
[25] M. Lyons, J. Budynek, A. Plante, S. Akamatsu, Classifying facial attributes using a 2-d Gabor wavelet representation and discriminant analysis, in: Intl. Conference on Automatic Face and Gesture Recognition, 28–30 March, 2000, pp. 202 – 207.
[26] K. Messer, J. Kittler, J. Short, G. Heusch, F. Cardinaux, S. Marcel, Y. Rodriguez, S. Shan, Y. Su, W. Gao, X. Chen, Performance characterisation of face recognition algorithms and their sensitivity to severe illumination changes, in: International Conference on Biometrics, ICB 2006, Hong Kong, China, January 5–7, 2006.
[27] A. Mian, M. Bennamoun, R. Owens, An efficient multimodal 2D–3D hybrid approach to automatic face recognition, IEEE Transactions on Pattern Analysis and Machine Intelligence 29 (11) (2007) 1927–1943.
[28] I. Mpiperis, S. Malassiotis, M.G. Strintzis, 3-d face recognition with the geodesic polar representation, IEEE Transactions on Information Forensics and Security 2 (3) (2007) 537–547.
[29] P.J. Phillips, P.J. Flynn, T. Scruggs, K.W. Bowyer, J. Chang, K. Hoffman, J. Marques, J. Min, W. Worek, Overview of the face recognition grand challenge, in: Proc. of CVPR05, June 2005, pp. 947–954.
[30] W. Press, S. Teukolsky, W. Vetterling, B. Flannery, Numerical Recipes in C: The Art of Science Computing, Cambridge University Press, 2008.
[31] S. Rizvi, P. Phillips, H. Moon, The FERET verification testing protocol for face recognition algorithms, in: Third IEEE International Conference on Automatic Face and Gesture Recognition, Nara, Japan, 14–16 April, 1998, pp. 48–53.
[32] H.-C. Shin, S.-D. Kim, H.-C. Choi, Generalized elastic graph matching for face recognition, Pattern Recognition Letters 28 (9) (2007) 1077–1082.
[33] H.-C. Shin, J. Park, S.-D. Kim, Combination of warping robust elastic graph matching and kernel-based projection discriminant analysis for face recognition, IEEE Transactions on Multimedia 9 (6) (2007) 1125–1136.
[34] X. Tan, S. Chen, Z. Zhou, F. Zhang, Face recognition from a single image per person: a survey, Pattern Recognition 39 (9) (2006) 1725–1745.
[35] A. Tefas, C. Kotropoulos, I. Pitas, Using support vector machines to enhance the performance of elastic graph matching for frontal face authentication, IEEE Transactions on Pattern Analysis and Machine Intelligence 23 (7) (2001) 735–746.
[36] A. Tefas, C. Kotropoulos, I. Pitas, Face verification using elastic graph matching based on morphological signal decomposition, Signal Processing 82 (6) (2002) 833–851.
[37] M. Turk, A.P. Pentland, Eigenfaces for recognition, Journal of Cognitive Neuroscience 3 (1) (1991) 71–86.
[38] L. Wiskott, Phantom faces for face analysis, Pattern Recognition 30 (6) (1997) 837–846.
[39] L. Wiskott, J. Fellous, N. Krüger, C.v.d. Malsburg, Face recognition by elastic bunch graph matching, IEEE Transactions on Pattern Analysis and Machine Intelligence 19 (7) (1997) 775–779.
[40] R.P. Würtz, Object recognition robust under translations, deformations, and changes in background, IEEE Transactions on Pattern Analysis and Machine Intelligence 19 (7) (1997) 769–775.
[41] S. Zafeiriou, M. Petrou, Nonlinear non-negative component analysis algorithms, IEEE Transactions on Image Processing 19 (4) (2010) 1050–1066.
[42] S. Zafeiriou, I. Pitas, Discriminant graph structures for facial expression recognition, IEEE Transactions on Multimedia 9 (10) (2008) 1528–1540.
[43] S. Zafeiriou, A. Tefas, I. Buciu, I. Pitas, Exploiting discriminant information in nonnegative matrix factorization with application to frontal face verification, IEEE Transactions on Neural Networks 17 (3) (2006) 683–695.
[44] S. Zafeiriou, A. Tefas, I. Pitas, Elastic graph matching versus linear subspace methods for frontal face verification, in: International Workshop on Nonlinear Signal and Image Processing, 2005.
[45] S. Zafeiriou, A. Tefas, I. Pitas, Exploiting discriminant information in elastic graph matching, in: Proc. of IEEE International Conference on Image Processing (ICIP 2005). Genova, Italy, September 11–14, 2005.
[46] S. Zafeiriou, A. Tefas, I. Pitas, The discriminant elastic graph matching algorithm applied to frontal face verification, Pattern Recognition 40 (10) (2007) 2798–2810.
[47] S. Zafeiriou, A. Tefas, I. Pitas, Learning discriminant person specific facial models using expandable graphs, IEEE Transactions on Information Forensics and Security 2 (1) (2007) 50–55.
[48] J. Zhang, Y. Yan, M. Lades, Face recognition: Eigenface, elastic matching, and neural nets, Proceedings of the IEEE 85 (9) (1997) 1423–1435.
[49] Z. Zhang, M. Lyons, M. Schuster, S. Akamatsu, Comparison between geometry-based and Gabor-wavelets-based facial expression recognition using multi-layer perceptron, in: Intl. Conference on Automatic Face and Gesture Recognition. Nara, Japan, 14–16, 1998, pp. 454–459.
[50] L. Zou, S. Cheng, Z. Xiong, M. Lu, K.R. Castleman, 3-d face recognition based on warped example faces, IEEE Transactions on Information Forensics and Security 2 (3) (2007) 513–528.